ADVANCED MATERIALS
www.advmat.de

Metal–Organic Framework Nanoparticles

*Shunzhi Wang, C. Michael McGuirk, Andrea d'Aquino, Jarad A. Mason, and Chad A. Mirkin**

Due to their well-defined 3D architectures, permanent porosity, and diverse chemical functionalities, metal–organic framework nanoparticles (MOF NPs) are an emerging class of modular nanomaterials. Herein, recent developments in the synthesis and postsynthetic surface functionalization of MOF NPs that strengthen the fundamental understanding of how such structures form and grow are highlighted; the internal structure and external surface properties of these novel nanomaterials are highlighted as well. These fundamental advances have resulted in MOF NPs being used as components in chemical sensors, biological probes, and membrane separation materials, as well as building blocks for colloidal crystal engineering.

1. Introduction

Metal–organic frameworks (MOFs), also known as porous coordination polymers, are 3D ordered porous materials composed of inorganic clusters bridged by organic ligands, which, in certain cases, exhibit record-setting internal surface areas.[1] Through judicious choice of organic and inorganic components, the crystalline structure and chemical functionalities of MOFs can be deliberately modulated, which has led to their use in a wide range of applications, including gas storage and separations,[2] chemical sensing,[3] membranes,[4] catalysis,[5] and drug delivery.[6] Since their discovery, the vast majority of MOF studies have focused on bulk phases composed of polydisperse mixtures of crystallites that span multiple orders of magnitude in size, however, more recently, significant effort has been dedicated toward the realization of uniform MOF nanoparticles (NPs), leading to the discovery of a variety of properties not observed or relevant in bulk systems, such as accelerated adsorption/desorption kinetics and improved bioavailability.[7] Indeed, ways of preparing uniform MOF NPs are critical to expanding our understanding of MOF structure–function relationships and applications based upon the unusual properties of such structures.

In contrast with conventional inorganic and organic NPs, for which syntheses and postsynthetic functionalization procedures are well established, the development of generalizable and mechanistically understood methodologies for MOF NP synthesis is still in its infancy. The ability to rapidly and reproducibly synthesize MOF NPs of uniform size and well-defined surface chemistry is highly desirable, as precise control over these factors is not only critical to the understanding of structure–function relationships, but also has significant impact on porosity,[8] catalytic activity,[9] and cellular uptake.[10] Indeed, it was not until inorganic and organic NPs could be reliably synthesized in monodisperse form and with controlled surface chemistry that their potential as applied materials and nanoscale building blocks could be realized.[11] At present, a large variety of inorganic NPs can be routinely synthesized with a coefficient of variation (CV) of less than 5%, whereas MOF NPs have only been achieved with a limited number of canonical frameworks, and often suffer from undesirable large size distributions (CV = 10–30%).[7b,12] In order to realize the full potential of MOF NPs, a firm understanding of the mechanisms underlying NP syntheses and methodologies for postsynthetic surface functionalization must be established.[13] In order to address this challenge, recent effort has been devoted toward elevating the study of MOF NPs to similar standards of rigorous characterization,[14] mechanistic understanding,[15] and chemical control that are characteristic of their purely inorganic and organic nanomaterial counterparts.[12,13]

Herein, we provide a perspective on two key areas of MOF NP research: 1) synthetic strategies for obtaining uniform MOF NPs with low size and shape dispersity (**Scheme 1**a), and **2**) postsynthetic functionalization of the external surfaces of MOF NPs (Scheme 1b). We conclude by highlighting opportunities that are emerging from the modular synthesis and postsynthetic modification of MOF NPs. Above all, the goal of this progress report is to highlight a selection of recent work that will provide readers with a synthetic toolbox for the design of MOF NPs that can be predictably tailored for desired applications. It should be noted that this article is not intended to provide a comprehensive survey of all MOF NP research to date, and we refer the interested readers to several comprehensive reviews on MOF nanostructures and their applications.[7b,12,16]

S. Wang, Dr. C. M. McGuirk, A. d'Aquino, Dr. J. A. Mason, Prof. C. A. Mirkin
Department of Chemistry and International Institute for Nanotechnology
Northwestern University
2145 Sheridan Road, Evanston, IL 60208, USA
E-mail: chadnano@northwestern.edu
Dr. C. M. McGuirk
Department of Chemistry
University of California
Berkeley, CA 94720, USA
The ORCID identification number(s) for the author(s) of this article can be found under https://doi.org/10.1002/adma.201800202.

DOI: 10.1002/adma.201800202

2. Synthesis of MOF NPs

Although syntheses of nanoscale MOF crystallites have been reported, the reliable preparation of uniform NPs remains a significant challenge.[12] For one, the thermodynamics of MOF formation can vary significantly for different metal–ligand combinations and framework topologies, thus synthetic methodologies must often be tailored for each individual framework. Kinetically, the formation of the relatively weak coordination bonds that drives MOF NP growth is typically slow (timescale of seconds) relative to the precursor diffusion rate in solution,[17] leading to extended periods of homogeneous nucleation and a broad particle size distribution.[15c,18] These variable contributions result in complex NP nucleation and growth processes that can be difficult to separate and independently control, including a number of mechanistic considerations not encountered in metallic NP analogs, such as linker deprotonation, solvent decomposition, and the formation of secondary building units (SBUs).[19]

These challenges have prompted extensive analytical studies of the mechanisms of MOF NP nucleation and growth. In particular, extended X-ray absorption fine structure,[19] time-resolved static light scattering,[15a] small- and wide-angle X-ray scattering,[15b] liquid cell transmission electron microscopy (LCTEM),[15c] and high resolution TEM have aided in this effort.[15d] As a consequence of these studies, the LaMer model of NP growth has been invoked as a primary tool for understanding MOF NP formation.[20] According to the LaMer model, the process of nucleation and growth occurs in four successive steps: 1) a rapid increase in the concentration of reactive monomers in solution (Scheme 2, stage I), 2) a homogeneous nucleation "burst" as the concentration of reactive monomers exceeds the critical nucleation concentration (C_{nuc}), 3) a rapid reduction in the concentration of monomers in solution, halting further nucleation events (Scheme 2, stage II), and 4) extended crystal growth upon reaching the saturation concentration (C_{sat}, i.e., the concentration at which the NP growth rate equilibrates with the solvation rate) (Scheme 2, stage III). The short nucleation period of the LaMer mechanism, which temporally separates crystal nucleation from crystal growth, is critical for the synthesis of uniform NPs. To obtain small, uniform (10–100 nm) MOF NPs (Scheme 2, blue trace), it is essential to generate a large number of nuclei via burst nucleation, and then to rapidly terminate particle growth through depletion of all precursors. However, to obtain large (200 nm–1 µm) MOF NPs (Scheme 2, red trace), slow particle nucleation and growth are needed to limit the number of nucleation sites, such that all precursors will react with fewer nuclei to form larger particles. To control these underlying factors and therefore NP size, most MOF NPs are synthesized via one of the following strategies, or some combination thereof: 1) rapid nucleation, 2) nanoreactor confinement, and/or 3) coordination modulation.

Chad A. Mirkin is a chemist and nanoscience expert, known for the invention of spherical nucleic acids, dip-pen nanolithography, and related cantilever-free, scanning-probe-based nanopatterning methodologies, and contributions to supramolecular chemistry and nanoparticle synthesis.

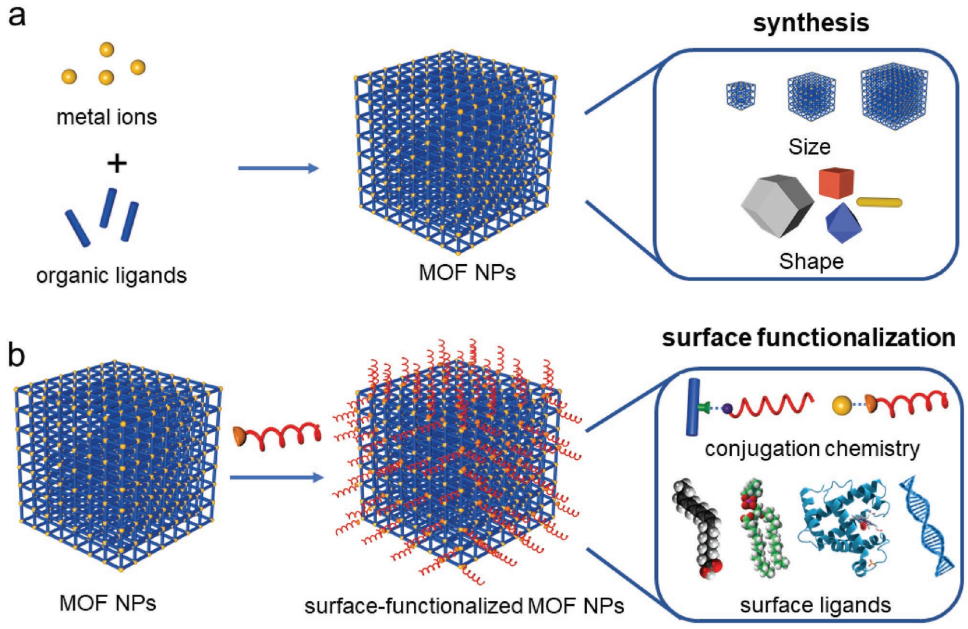

Scheme 1. Schematic representation of (a) the modular synthesis of MOF NPs, with control over size and morphology, and (b) the postsynthetic external surface functionalization with multiple conjugation strategies and types of surface ligands.

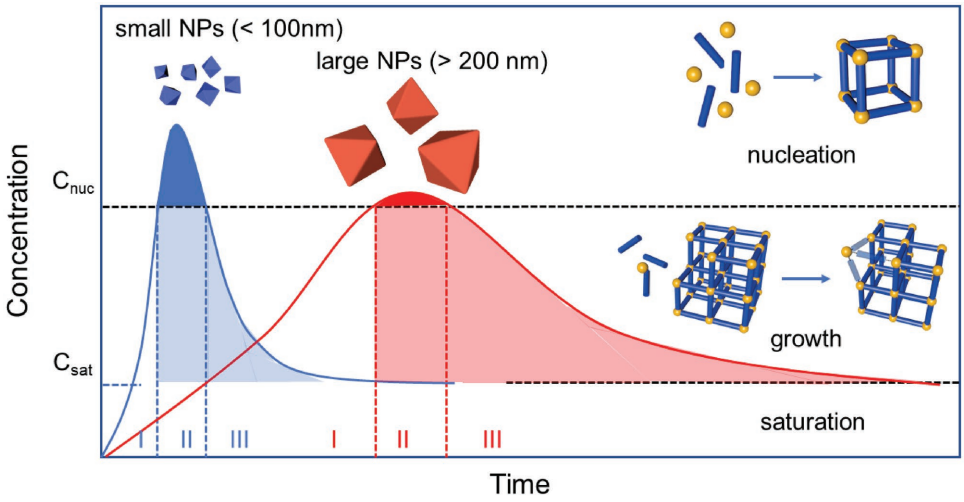

Scheme 2. Schematic representation of MOF NP nucleation and growth according to the LaMer model. Blue trace, the synthesis of uniform small MOF NPs typically involves fast formation of abundant nuclei. Red trace, a small number of nuclei and slow growth rate results in uniform large NPs.

2.1. Rapid Nucleation

Before the realization of crystalline MOF NPs, much of the early work on nanoscale inorganic–organic hybrid materials focused on amorphous coordination polymers (CPs). Although analogously composed of tailorable ligands and metal cations, these systems lack long-range structural order and permanent porosity. Nonetheless, nanoscale amorphous CPs served as an important predecessor in the development of crystalline MOF NPs.[16a,21] Taking advantage of solubility differences between molecular precursors and the resulting polymer particulates, CP NPs were typically synthesized through manipulation of precursor concentration, pH of the reaction mixture, or introduction of precipitating solvents. For example, in 2005, Wang and co-workers reported the synthesis of 300 nm spherical CP NPs derived from a mixture of H_2PtCl_6 and *p*-phenylenediamine in aqueous solution at room temperature.[22] The NP size and polydispersity were controlled by the molar ratio and concentration of reactants. Separately, Oh and Mirkin pioneered an "initiation-solvent" approach, whereby the controlled introduction of a secondary initiation antisolvent into the homogeneous precursor solution led to the formation of amorphous M-BMSB NPs (M = Zn^{2+}, Cu^{2+} and Ni^{2+}; BMSB = bis-metallo-tridentate Schiff base) (**Figure 1**b).[23] Particle sizes were reduced from 2 µm to 190 nm (CV = 20–30%) via fast addition of initiation solvent, however, the resulting particles were relatively polydisperse. In some cases, the simple mixing or addition of initiation solvent alone is not sufficient to induce fast nucleation, and base can be added to deprotonate acidic proligands and accelerate initial coordination events. Indeed, Lin and co-workers improved upon the initiation-solvent method by deprotonating precursor ligands to accelerate nucleation rates, leading to the formation of 58 ± 8 nm (CV ≈ 15%) $Tb_2(DSCP)_3(H_2O)_{12}$ (DSCP = disuccinatocisplatin)

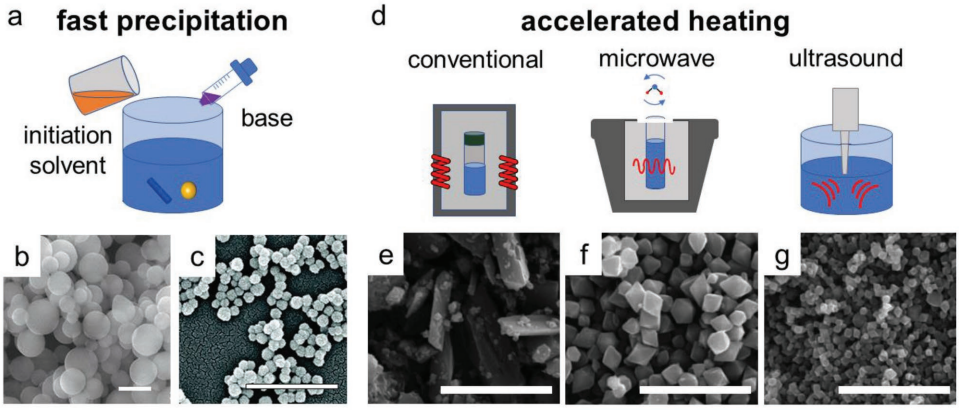

Figure 1. a) Schematic representation of CP NPs synthesized by the fast precipitation method. b) Scanning electron microscopy (SEM) image of spherical Zn-BMSB CP NPs synthesized via initiation-solvent approach. Scale bar = 200 nm. Reproduced with permission.[23] Copyright 2005, Nature Publishing Group. c) SEM image of spherical $Tb_2(DSCP)_3(H_2O)_{12}$ CP NPs synthesized via the deprotonation method. Scale bar = 500 nm. Reproduced with permission.[24] Copyright 2008, American Chemical Society. d) Schematic representation of MIL-53 MOF NPs synthesized by three different heating methods and their corresponding SEM images: e) conventional electric heating, (f) microwave, and (g) ultrasound. Scale bar = 10 µm. Reproduced with permission.[31] Copyright 2010, Wiley-VCH.

NPs (Figure 1c).[24] Interestingly, these CP NPs composed of Tb^{3+} and a Pt(IV) prodrug were shown to be an effective anticancer therapeutic agent. To date, a variety of amorphous CP NPs have been synthesized via the rapid precipitation strategy; however, few examples of uniform crystalline frameworks synthesized in this fashion exist, as rapid NP formation at room temperature precludes the necessary high degree of reversible bond formation achieved under solvothermal conditions for the realization of crystalline order.[12,65] Therefore, alternative synthetic approaches that promote reversible metal–ligand coordination bond formation are critical for the synthesis of uniform crystalline MOF NPs.

In this vein, accelerated heating is an important strategy for achieving rapid nucleation of crystalline NPs. Due to its fast heating, uniform energy generation throughout the bulk of the material, and ability to exceed the boiling point of a solvent through the use of pressurized vessels, microwave heating has been broadly applied as a tool for the realization of concentrated and small nuclei, which rapidly consume precursors and produce NPs with relatively narrow size distributions.[25] In 2006, Masel and co-workers[26] performed the first microwave-assisted solvothermal synthesis of MOF NPs. Cubic $Zn_4O(BDC)_3$ (IRMOF-1/MOF-5, BDC = 1,4-benzenedicarboxylate) NPs, ranging from 4 μm to 200 nm in edge length (CV ≈ 30%), were synthesized by reducing reactant concentrations. Notably, NPs were synthesized in less than a minute, whereas conventional heating takes tens of hours. Building on this initial work, much attention has focused on extending this technique to a variety of canonical frameworks. For example, Serre and co-workers optimized the synthesis of sub-100 nm uniform $Fe_3O(H_2O)_3(fum)_3$ NPs (Fe-MIL-88A, fum = *trans*-butenedioic acid) (CV < 10 %).[27] In this study, the authors systematically investigated synthetic parameters that control MOF NP size, including precursor concentration, reaction time, and temperature. Furthermore, Feldhoff and co-workers reported the microwave-assisted synthesis of $Zn(PhIm)_2$ (zeolitic imidazolate framework-7 (ZIF-7), PhIm = benzimidazolate) NPs, in which diethylamine was added to further accelerate the nucleation rate, promoting a series of NPs ranging from 40 to 140 nm (CV = 10–20%).[28]

In addition to microwave-based heating, ultrasound has been demonstrated as a useful tool for accelerating precursor dissolution and nucleation. Ultrasound effects originate from acoustic cavitation which generates local hot spots (ring of ≈200 nm) with transient high temperature (≈5000 K), high pressure (>1000 bar), and rapid heating and cooling rates.[29] The nucleation and growth of particles preferably occurs in these transient hot spots (within milliseconds), effectively limiting particle size to the nanoscale.[30] In a comprehensive kinetic study of Fe(OH)BDC (MIL-53-Fe) NP crystallization, Jhung and co-workers studied how microwave, ultrasound, and conventional electric heating methods can drastically affect MOF nucleation and growth kinetics (Figure 1d–g).[31] In this study, the temperature was kept constant across heating methods, and the reaction time was varied to investigate the crystallization process. The authors found that crystal growth rates were comparable across all the three methods, however MOF NP size inversely correlated with nucleation rate (conventional heating << microwave < ultrasound), and that uniform, geometrically defined NPs were only obtained from microwave and ultrasound syntheses. This study provided direct evidence that the methods used to promote rapid nucleation, namely heating rates and temperature profiles within reaction containers, have a significant impact on particle size and uniformity. It should be noted that although ultrasound irradiation provides the fastest heating acceleration, it often suffers from relatively low yield, poor temperature control, and the formation of mixed-phase frameworks.[32] Because of these challenges, microwave-assisted synthesis has been more widely adopted.[6,27,33]

2.2. Nanoreactor Confinement

Different from burst nucleation via rapid precipitation or accelerated heating, nanoreactor confinement strategies regulate MOF NP size via the isolation of nucleation sites in a physically confined space. In this approach, immiscible solvents, such as water and "oil" (a complex mixture of different hydrocarbons and olefins), are mixed to produce emulsions of monodisperse nanoscale droplets, and both the emulsion size and reagent solubility can be tuned by varying the concentration of amphiphilic surfactants (**Figure 2**a).[34] In the presence of MOF precursors, these droplets serve as size-limiting reaction containers, in which particle nucleation kinetics are controlled by emulsion size, rate of mixing, and reaction temperature.[12] It is important to recognize that these microemulsion systems are dynamic, with micelles frequently colliding and coalescing, allowing reagents solubilized in separate micellar solutions to mix and react. Subsequently, at the latter stage of particle growth, steric stabilization provided by the surfactant layer prevents NPs from aggregating.

Lin and co-workers first synthesized crystalline nanorods of $Ln_2(BDC)_3(H_2O)_4$ (Ln = Eu^{3+}, Gd^{3+}, or Tb^{3+}) by reacting $LnCl_3$ and bis(methylammonium)-BDC in an emulsion system composed of isooctane/1-hexanol/water and varying the amount of the surfactant cetyltrimethylammonium bromide (CTAB).[35] By varying the ratio of water to surfactant from 10:1 to 5:1, the size of the nanorods could be tuned from 2 μm × 100 nm to 125 nm × 40 nm (Figure 2b,c), where emulsions with higher water:surfactant ratios yielded MOF NPs with higher aspect ratios. Additionally, the average particle size decreased as reactant concentrations increased, presumably because more micelles contained reactants and thus more nucleation sites were generated, leading to a reduction in particle size. Such a reverse-phase microemulsion (water-in-oil) was extended to synthesize a series of Mn-based MOF NPs. Nanorods of $Mn(BTC)_2(H_2O)_6$ (BTC = benzene-1,3,5-tricarboxylic acid, with diameters of 50–100 nm and lengths of 750 nm to several micrometers) were synthesized in a CTAB/1-hexanol/*n*-heptane/water microemulsion containing equal molar $MnCl_2$ and bis(methylammonium)-BDC.[36] Notably, as the reaction temperature increased from room temperature to 120 °C, the aspect ratio of the NPs decreased dramatically (Figure 2d,e). Recently, Zheng and co-workers synthesized $Zn(mIM)_2$ (ZIF-8, mIM = 2-methylimidazolate) NPs with narrow size distribution using reverse-phase micelles (CV < 10%).[37] By tuning the precursor concentration, reaction temperature, and surfactant species, NP sizes were modulated between 30 and 300 nm, which in turn demonstrated distinct size-dependent catalytic activity

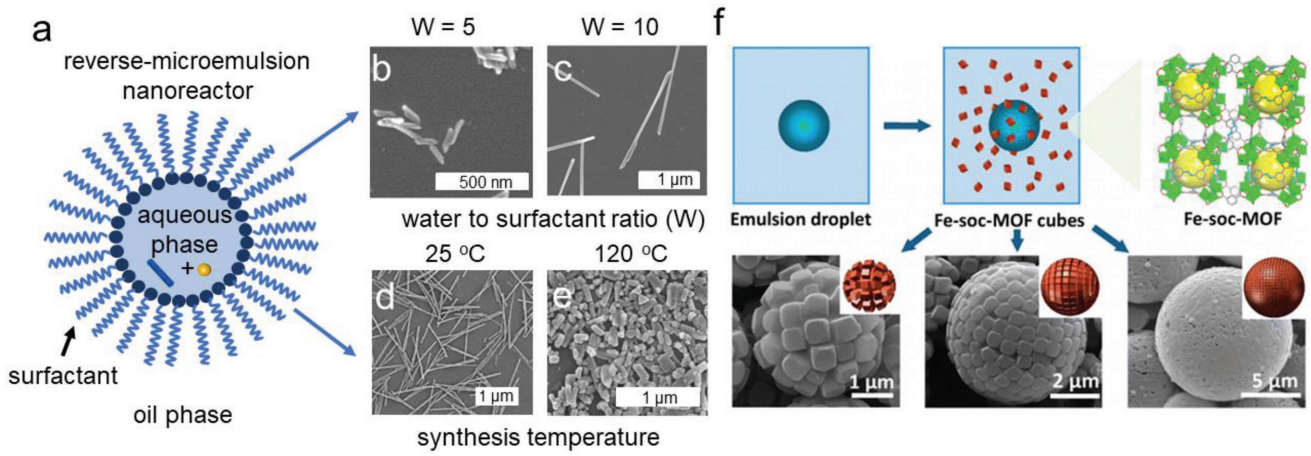

Figure 2. a) Schematic representation of a reverse-phase microemulsion serving as a nanoreactor for MOF NP syntheses. b,c) SEM images of $Ln_2(BDC)_3(H_2O)_4$ particles synthesized at different water to surfactant ratios which effect the resulting aspect ratio. Reproduced with permission.[35] Copyright 2006, American Chemical Society. d,e) SEM images of $Mn(BTC)_2(H_2O)_6$ particles synthesized at different temperatures where lower aspect ratios and smaller size result from higher temperature. Reproduced with permission.[36] Copyright 2008, American Chemical Society. f) Schematic representation of synthesis and integration of Fe-soc-MOF cubes into hollow colloidosomes and the corresponding SEM images. Reproduced with permission.[38a] Copyright 2013, American Chemical Society.

for a Knoevenagel condensation reaction. Further, Eddaoudi and co-workers reported an emulsion-templating approach to prepare cubic $[Fe_3O\text{-}(ABTC)_{1.5}(H_2O)_3](H_2O)_3(NO_3)$ MOF NPs (Fe-soc-MOF, H_4ABTC = 3,3′,5,5′-azobenzenetetracarboxylic acid).[38] Notably, due to the high uniformity of Fe-soc-MOF NPs and the presence of emulsion droplet induced by polyoxyethylene (20) sorbitan trioleate (tween-85) surfactant, these cubic MOF NPs self-assembled into hollow colloidosomes during the one pot synthesis (Figure 2f). The relative size of the hollow colloidosomes is dependent upon the size of emulsion droplets, which inversely correlates with the concentration of tween-85. Inspired by conventional emulsion methods, Maspoch and co-workers developed a novel and general spray-drying technique to synthesize MOF NPs.[39] This approach conceptually mimics the emulsion strategy that confines the synthesis of materials, but does not require secondary immiscible solvents or surfactants as templates. In a typical synthesis, droplets containing MOF precursors are vaporized via spraying and then heated, leading to sub-5 μm hollow spherical superstructures with localized crystallization of MOF NPs at the droplet–air interface.[40] The disassembly of the superstructures by sonication yields discrete but nonuniform MOF NPs. In general, the microemulsion approach provides an effective way to regulate MOF NP size and to reduce size distribution; however, drawbacks exist, including: 1) relatively low yields, 2) poor reproducibility associated with complicated micelle formation and droplet coalescence processes, and 3) harsh conditions or multiple washing steps to completely remove all surfactants and organic solvents. These challenges potentially limit the practical use of MOF NPs in biomedical applications.

2.3. Coordination Modulation

Coordination modulation is a general approach to regulate MOF NP synthesis via chemically controlling ligand–metal interactions, which can be applied in conjunction with rapid nucleation and nanoreactor confinement strategies. Coordination modulators are primarily monotopic (i.e., nonbridging) ligands that are added to the reaction mixture to either affect linker deprotonation equilibria or reversibly compete with bridging linkers for available metal ion/cluster coordination sites.[41] Chemical modulators are able to impact NP size and shape by controlling the number of nucleation sites produced and preferentially binding to certain crystal facets (**Figure 3**a). Indeed, the pK_a, steric profile, and concentration of such modulators are variable properties that play crucial rules in regulating particle size, shape, and uniformity.[42]

In an early exploration of the effect of modulators on amorphous CP NP growth, Kitagawa and co-workers demonstrated the size modulating effect of poly(vinylpyrrolidone) (PVP), a weakly coordinating polytopic polymer, on Prussian blue NP formation.[43] The authors reported that the use of this competitive ligand produced a significant reduction in particle size, from 300 to 16 nm, along with improved size uniformity. Fischer and co-workers further demonstrated size control for crystalline MOF-5 NPs by influencing the particle nucleation rate via the addition of *p*-perfluoro-ethylbenzoic acid modulator.[15a] In addition to size control, shape control has also been achieved via coordination modulation by employing surfactant/blocking/capping agents that interact with specific crystal facets, deterring particle growth in that direction. For example, Oh and co-workers discovered that the aspect ratio of In(OH)(BDC) hexagonal nanorods can be controlled from 0.11 to 0.91, by increasing the amount of pyridine.[44] The authors postulated that in the presence of excess pyridine, particle growth in the direction of the hexagonal facets is effectively blocked, resulting in hexagonal disks. In a more straightforward system, Kitagawa and co-workers studied the modulated growth of pillar-layered MOF $Cu_2(ndc)_2(dabco)$ (ndc = 1,4-naphthalene dicarboxylate; dabco = 1,4-diazabicyclo[2.2.2]octane) NPs, which feature two separate coordination modes: Cu–ndc (carboxylate) to form 2D

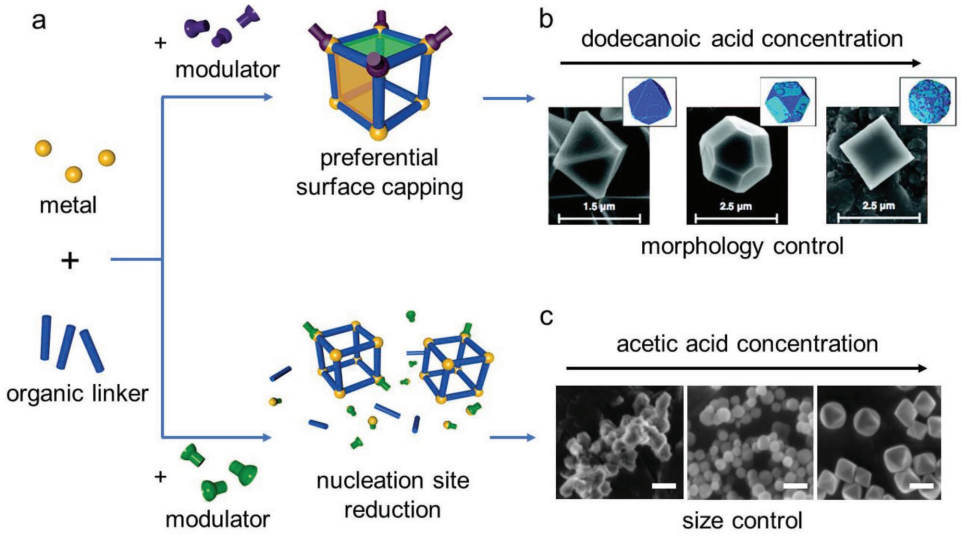

Figure 3. a) Schematic illustration of coordination modulation strategy impacting NP shape by selectively binding to specific crystal facets, and crystallite size by controlling the number of nucleation sites produced. b) SEM images showing morphology of HKUST-1 NPs transitioning from octahedra to cuboctahedra to cube as the dodecanoic acid modulator concentration increases. Reproduced with permission.[46] Copyright 2011, American Chemical Society. c) SEM images of UiO-66 NPs showing that particle size positively correlates with increasing acetic acid modulator concentration. Scale bar = 200 nm. Reproduced with permission.[50] Copyright 2011, Wiley-VCH.

sheets and Cu–dabco (amine) to bridge the 2D sheets.[45] By adding an acetic acid modulator, square-rod anisotropic NPs were selectively formed due to Cu–acetic acid coordination on the (100) surface, which induces selective crystal growth along the [001] direction. Following up on this work, control over the crystal morphology of $Cu_3(BTC)_2$ (Hong Kong University of Science and Technology (HKUST)-1) particles was achieved by simultaneously tuning the concentration of the two modulators, acetic and dodecanoic acids.[46] In particular, by varying the dodecanoic acid concentration from 0.234 to 1.188 M, HKUST-1 particles were synthesized with a crystal morphology transitioning from nanoscale octahedra to micrometer-sized cuboctahedra to micrometer-sized cubes (Figure 3b). By employing coarse-grained modeling, the authors suggested that the preferential capping of the modulator at certain nucleation sites was dictated by differences in the relative crystal facet surface energy, leading to different morphologies. In addition to modulating crystal morphology during solvothermal synthesis, postsynthetic etching strategies also have been realized.[47] For example, Maspoch and co-workers demonstrated the surface-selective anisotropic etching of ZIF-8 and ZIF-67 ($Co(mIM)_2$) NPs via ligand protonation and subsequent metal ion sequestration.[48] Specifically, the addition of xylenol orange, a weak acid and metal sequestering agent, protonates the 2-mIM linkers, breaking the Zn/Co−2-mIM bonds and preferentially etching the external crystal surfaces with the highest density of Zn/Co−2-mIM bonds. By adjusting the pH of the xylenol orange solution, the morphology of ZIF NPs can be converted from rhombic dodecahedra to hollow boxes. The ability to control crystal morphology represents a significant advancement, as the predictable exposure of certain crystal facets allows control over surface reactivity and diffusion kinetics.[49]

More recently, significant attention has been given to the synthesis of zirconium-based MOFs, such as the UiO (University of Oslo) and PCN (porous coordination network) families, due to their exceptional stability in aqueous solutions—a desirable property for many biological applications. In prototypical bulk syntheses of $Zr_6O_4(OH)_4(BDC)_6$ (UiO-66), the fast kinetics and low reversibility of bond formation between highly oxophilic Zr^{4+} salts and the terephthalic acid linker precludes control over particulate size and morphology. Therefore, the development of chemical modulators that effectively slow down the reaction and increase reversibility are highly desirable for the synthesis of homogeneous crystalline Zr MOF NPs. In this vein, Behrens and co-workers first reported that benzoic and acetic acids could be used as modulators in the size-controlled synthesis of Zr-based UiO-66 and UiO-67 NPs (Figure 3c).[50] The addition of these monotopic acids led to the initial formation of Zr–modulator coordination complexes, where the modulators were slowly replaced by ditopic linker molecules to form the frameworks. Such exchange equilibrium provided control over crystallization rates (especially nucleation rates) and changed the product morphology from aggregates of intergrown crystallites to individual NPs. With this understanding, Zhou and co-workers[10] systematically controlled the size of $Zr_6O_4(OH)_4(TCPP\text{-}H_2)_3$ (PCN-224/MOF-525, TCPP = tetrakis(4-carboxyphenyl)porphyrin) NPs with benzoic acid. They reported a series of uniform MOF NPs, ranging from 33 ± 4 to 189 ± 11 nm, which allowed for the evaluation of size dependence on cellular uptake and subsequent use in photodynamic therapy efficacy. In addition to size and morphology, the pK_a of the acidic modulator can be leveraged to control UiO-66 NP porosity,[51] surface charge, colloidal stability, and size dispersity.[52]

The use of chemical modulators has led to some of the most uniform MOF NPs (CV ≈ 5%) reported to date, which has enabled the exploration of incorporating these materials into higher ordered structures. In such cases, chemical

modulators often not only control NP growth, but also serve as surfactants that manipulate NP surface properties and facilitate self-assembly processes. For example, the Langmuir–Blodgett technique has been employed to prepare 2D monolayer films of $Al_{12}O(OH)_{18}(H_2O)_3(Al_2(OH)_4)(BTC)_6$, $[M_3O\text{-}(C_{16}N_2O_8H_6)_{1.5}(H_2O)_3](H_2O)_3(NO_3)$ (M-soc-MOF, M = In and Ga), and UiO-66 NPs.[53] Further, Granick and co-workers synthesized homogeneous PVP-coated ZIF-8 NPs (CV ≈ 4.5%) and showed that these rhombic dodecahedron particles assemble into interesting structures driven either by capillary forces or an applied external electric field.[54] Recently, Maspoch and co-workers elegantly demonstrated CTAB-mediated self-assembly of uniform polyhedral ZIF-8 and UiO-66 NPs (≈200 nm with CV ≈ 5%) into millimeter-sized 3D photonic materials.[55] These superstructures feature a photonic bandgap that can be tuned by controlling the size of the NPs and are responsive to the adsorption of guest molecules in the MOF pores, providing a glimpse into potential sensing applications.

Overall, coordination modulation has emerged as the most versatile and effective strategy for synthesizing highly uniform MOF NPs with narrow size distribution. However, it should also be noted that, at present, the choice of modulator greatly relies on empirical knowledge and size and morphology control are achieved by changing the conventional solvothermal reaction conditions in a trial-and-error fashion. Therefore, it is highly desirable to improve upon this approach with the development of high-throughput synthetic screening and characterization methodologies to effectively identify and evaluate the optimal modulator species, reagent concentration, as well as reaction temperature and time for synthesizing diverse, high quality MOF NPs.[56]

3. Surface Functionalization of MOF NPs

Surface ligands play a critical role in dictating the chemical and physical properties of nanomaterials.[11] Indeed, properties such as solubility, cellular uptake, molecular recognition, and catalytic reactivity can be postsynthetically modulated by surface ligands. This tailorability has proven to be important for the realization of many promising applications, including drug delivery, light-induced catalysis, and self-assembly.[57] Similar to inorganic and organic NPs, the as-synthesized MOF NPs often exhibit unfavorable surface properties, such as limited colloidal stability and poor bioavailability/pharmacokinetics.[16d] Therefore, postsynthetic modification (PSM) of the external surface of MOF NPs has been proposed as a generalizable tool for mitigating these concerns and imbuing MOF NPs with desired functionality, such as enhanced colloidal stability, stimuli-responsive guest release, improved cellular uptake, and biomarker targeting.[58] Specifically, polymers and biomacromolecules, including lipids, peptides, and nucleic acids, are particularly attractive choices as surface ligands, owing to their exceptional chemical tailorability and steric inability to diffuse into the pores of most MOFs, limiting functionalization to the external surface. Although various approaches have been reported for PSM of MOF NPs, we have chosen to focus on those that occur through direct bonding interactions between ligands and the NP's external surface. Below, we highlight two important external surface PSM strategies, which vary in the bonding mode at the ligand–NP interface, namely: 1) covalent surface functionalization, and 2) coordinative surface functionalization (**Scheme 3**). We discuss the relative advantages and disadvantages of the two approaches and their potential applications. It should be noted that much effort has been devoted to developing nonspecific interactions and encapsulation-based PSM strategies, however these approaches are challenging to quantify and tend to reduce MOF porosity; therefore, they will not be discussed in this review.

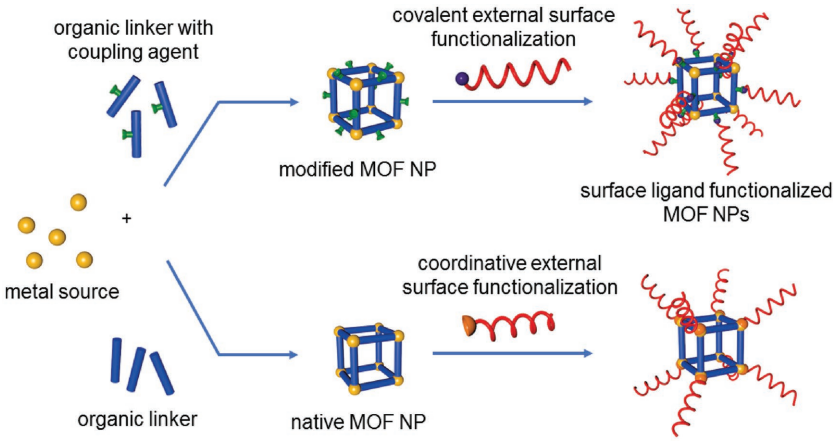

Scheme 3. Schematic illustration of postsynthetic modification of MOF NP external surfaces through covalent bonds (top) and coordinative bonds (bottom) at the SBUs.

3.1. Covalent External Surface Functionalization

Covalent PSM of substituted organic linkers is a robust and versatile strategy for imparting functionality to MOF NPs without interfering with the particle crystallization processes. This approach relies on the presynthetic installation of reactive functional groups onto the organic linkers of MOF NPs, which are reacted post-framework synthesis with exogenous ligands containing compatible organic units. Foresight into potential deleterious cross talk between linker and SBU is critical in this approach, as the installation of such reactive functional units can necessitate long and/or complex organic syntheses. As will be discussed below, these organic functional groups are typically amines, carboxylic acids, and azides, which are able to subsequently react with carbonyl, amine, and alkyne groups, respectively, installed on the exogenous ligand.[59] Below, we discuss a series of reports in which the external surface of MOF NPs are modified through the formation of organic covalent bonds between the linkers of the framework and secondary surface ligands.

Owing to the near ubiquity of carboxylic acid-based ligands, postsynthetic reactions at surface exposed, nonmetal bound

linker carboxylates were a logical starting point for PSM via organic covalent bonds. As an important note, early efforts required no additional functionalization of the native linker. Generally, carboxylate units on MOF NP surfaces were targeted for conjugation with primary amine bearing ligands or modified bio-macromolecular ligands such as peptides and proteins. For example, Park and co-workers first demonstrated the use of carbodiimide coupling agents to promote the conjugation of free carboxylate units on the bulk MOF surface with proteinaceous amines. Importantly, this approach retained the endogenous catalytic activity and enantioselectivity of the protein.[60] In 2012, Lin and co-workers covalently bound the protease trypsin onto free hanging carboxylate moieties of $Cr_3O(H_2O)_3(BDC{-}NH_2)_3$ [MIL-88B$-NH_2$(Cr)] via an endogenous terminal amino group using a similar carbodiimide-mediated coupling reaction, to afford a reusable bovine serum albumin digestion system.[61] In a demonstration of increased generality, Lei and co-workers employed 1-ethyl-3-(3-dimethylaminopropyl)-carbodiimide/*N*-hydroxysuccinimide (NHS) to graft the protein streptavidin to HKUST-1 and $Fe_3O(TCPP)_3$ (FeTCPP, $TCPP^{4-}$ = 4,4′,4″,4‴-(porphine-5,10,15,20-tetrayl)tetrakisbenzoate) MOF NPs for electrochemical DNA sensing.[62] In addition to peptides and proteins, poly(ethylene glycol) (PEG) is an important class of macromolecule that is routinely employed to functionalize NP surfaces. PEGylation effectively prevents nonspecific protein adsorption onto NP surfaces, promoting desirable biomedical applications, such as prolonged blood-circulation time and reduced immune response.[63] Wuttke and co-workers recently reported the functionalization of the surface of 150 nm $Fe_3F(H_2O)_2O(BTC)_2$ (MIL-100(Fe)) NPs with amino-PEG 5000 and Stp10-C, an oligoaminoamide hetero-bifunctional linker (**Figure 4**a).[64] Their study revealed that significantly enhanced colloidal stability and efficient dye labeling can be achieved, which are extremely important for exploring the biomedical applications of MOF NPs. Although these reports demonstrate the versatility of addressing unbound ligand units on MOF NP surfaces, limitations exist, such as relatively low density of surface functionalization.[16d] Additionally, reaction with the linker unit of the framework can cause orthogonality issues, as the labile surface metal–linker coordination bond may undergo dissociation or dynamic ligand exchange.[65]

In contrast to the previous approach, linker modification should yield a high density of reactive surface sites whose location and density can be predicted from the structure of the framework. Using this approach, Webley and co-workers showed that surface functionalization with hydrophilic PEG prevents NP aggregation and greatly improves colloidal stability in water.[66] Specifically, amino-functionalized $Zr_6O_4(OH)_4(BDC{-}NH_2)_6$ (UiO-66$-NH_2$) was first anchored with a polymerization initiator by reacting with bromoisobutyryl bromide, followed by the atom-transfer radical polymerization of the macromonomer poly(ethylene glycol) methyl ether methacrylate initiated from the MOF surface. The PEG-grafted MOFs obtained from this procedure showed excellent dispersity in aqueous solution. Using a chemically identical framework, Sada and co-workers reported the covalent attachment of the NHS-modified thermosensitive polymer poly(*N*-isopropylacrylamide) (PNIPAM-NHS).[67] The pores of PNIPAM-functionalized NPs were loaded with guest molecules and the hybrid material was shown to exhibit temperature-controlled guest release, arising from the coil–globule transition of the thermoresponsive polymer. Surface functionalization employing amino-modified linkers has become a generalizable approach to tune MOF NP surface chemistry; however, the installation of these linker modifications can be tedious and often requires additional coupling reagents. Therefore, specific and robust conjugation chemistries that operate under mild conditions have been sought extensively.

Owing to the near ubiquitous nature of the highly specific and chemically orthogonal Huisgen "click" reaction, azide- or alkyne-functionalized organic linkers have been extensively used for covalent PSM with a diverse array of organic units.[68] Recently, Mirkin and co-workers reported the preferential functionalization of oligonucleotides onto the surface of both infinite coordination polymer NPs and MOF NPs via a copper-free, strain-promoted azide–alkyne cycloaddition.[69] Azide-functionalized 15 and 500 nm $Zr_6O_4(OH)_4(BDC{-}N_3)_6$ (UiO-66$-N_3$)

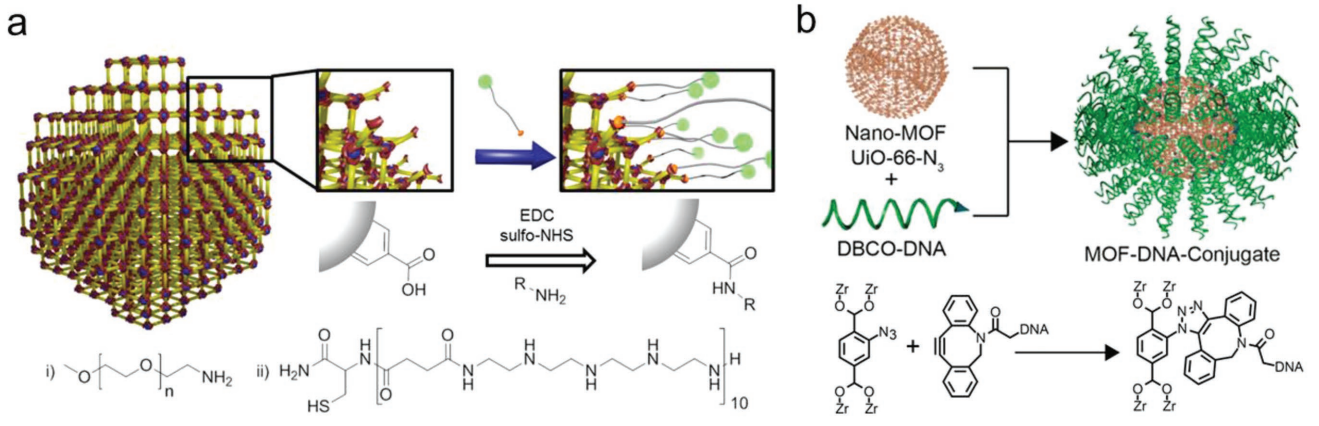

Figure 4. Schematic representation of postsynthetic external surface functionalization via different kinds of covalent bond formation: a) carbodiimide-catalyzed polymer and peptide surface functionalization of MIL-100-Fe MOF NPs with (i) amino-PEG 5000 and (ii) Stp10-C, respectively, and (b) oligonucleotide functionalization of UiO-66$-N_3$ MOF NPs with DBCO-modified DNA via click chemistry. Panel (a) reproduced with permission.[64] Copyright 2016, American Chemical Society. Panel (b) reproduced with permission.[69] Copyright 2014, American Chemical Society.

NPs were prepared and subsequently reacted with dibenzylcyclooctyne (DBCO)-terminated DNA (Figure 4b). Through this approach, the authors were able to achieve a sufficiently high surface coverage of DNA so as to imbue the MOF NPs with key properties previously observed for DNA-modified gold NPs. Namely: 1) improved colloidal stability, 2) participation in materials assembly via cooperative DNA hybridization, and 3) cellular uptake through endogenous endocytosis.[70] Through a slight modification of this approach, Willner and coworkers demonstrated how PSM of the reactive linker moiety can be leveraged to overcome synthetic hurdles.[71] Specifically, amino-functionalized $Zr_6O_4(OH)_4(TPDC{-}NH_2)_6$ (UiO-68, $TPDC{-}NH_2$ = 2′-amino-1,1′:4,1″-terphenyl-4,4″-dicarboxylic acid) NPs were reacted with *t*-butyl nitrite and trimethylsilyl azide to convert the linker amino unit into an azide functionality, which could then be "clicked" with DBCO-modified nucleic acids. This postsynthetic organic transformation was conducted due to synthetic incompatibilities associated with the installation of the desired azide unit before the framework was assembled. These nucleic acid-functionalized NPs were then used to realize two different stimuli-responsive materials in which specific stimuli induced the reconfiguration of the surface DNA gates, thus triggering the release of a molecular load stored in the framework pores. In addition to incorporating coupling agents via organic linker substitution, Forgan and coworkers reported an alternative approach based on decorating the framework with azide-functionalized modulators.[72] In this study, 200 nm UiO-66 MOF NPs were synthesized in the presence of acidic modulators containing azido or propargyl units (*para*-azidomethylbenzoic acid and *para*-propargyloxybenzoic acid) that attach to Zr_6 sites on UiO-66 NP surface, and thus allow for subsequent PEGylation via click chemistry. It was demonstrated that surface PEGylation endowed the NPs with enhanced stability toward phosphates and prevented undesirable "burst release" in drug delivery. Additionally, the cell-uptake behavior of these NPs could be altered, where increased caveolae-mediated endocytosis occurred for UiO-66 NPs functionalized with long chain PEGs (PEG 2000) as compared to short chain PEGs (PEG 550). Overall, these reports illustrate how surface functionalization, especially with nucleic acids and biocompatible polymers, can lead to the development of novel platforms with a multitude of applications in the biological sciences and medicine.[73]

Indeed, PSM via the formation of covalent organic bonds is a powerful tool for functionalizing the surface of MOF NPs with a diverse range of ligands, thus enhancing their desirable physical properties or endowing them with new chemical and biochemical properties. Nevertheless, this approach does have its drawbacks, namely: 1) ligand modification with reactive organic moieties is often synthetically challenging, 2) presynthetic linker modification permanently alters the inner pore environment of the resulting framework, leading to a reduction in porosity, and 3) many desirable covalent surface functionalization reactions require catalysts that may not be compatible with the framework or bio-macromolecule. With these potential complications in mind, we discuss an alternative approach that precludes the modification of organic linkers and potentially permits PSM of a broader scope of frameworks.

3.2. Coordinative External Surface Functionalization

The development of a generalizable methodology that obviates organic modification of the native framework is highly desirable, as this would maintain the innate bulk properties of the framework and preclude tedious linker syntheses. Intriguingly, MOF crystallites often contain a high density of surface metal sites that are weakly bound to nonbridging linkers or solvent molecules. It was therefore proposed that these accessible coordination sites could be harnessed as a place to postsynthetically anchor ligands that were functionalized with more strongly coordinating moieties. As these weakly coordinated surface sites are widely present in unmodified MOF NPs, external surface PSM via coordination bonds represents a generalizable approach to surface functionalization.[74] Compared to the covalent bond functionalization strategy, this metal–ligand coordination approach offers two powerful advantages: 1) straightforward synthesis without the use of coupling reagents or substituted linkers, and 2) applicability to all frameworks that are stable in the presence of coordinative surface ligands.[65] Therefore, a growing number of macromolecules, such as polymers, peptides, and oligonucleotides, have been functionalized with terminal coordinating groups for PSM of unmodified MOF NPs.

Kitagawa and co-workers first demonstrated this approach using carboxylate-terminated ligands for the functionalization of micrometer-scale Zn-based particles.[75] The authors were successful in functionalizing the particles with a monolayer of carboxylate-terminated boron-dipyrromethene (BODIPY) dye, however, elevated temperatures (120 °C) and long incubation times (48 h) were necessary due to the similar coordination strength of the two ligands being exchanged. More recently, Cha and co-workers demonstrated an elegant approach to functionalizing PCN-224 NPs, composed of Zr_6-based SBUs, with DNA.[76] PCN-224 NPs were first reacted with N_α,N_α-bis(carboxymethyl)-L-lysine hydrate, which contains three carboxylic acid functional groups that can coordinate cooperatively and strongly with the surface Zr sites, promoting facile surface ligand exchange and exposing a targetable alkyl amine group on the surface of the MOF. The amine-modified NPs were then functionalized with a NHS–DBCO linker via NHS–amine chemistry, which was followed by DNA conjugation with azido-terminated oligonucleotides. With the surface oligonucleotides installed, the MOF NPs were predictably assembled via hybridization with complementary DNA-modified upconversion NPs, leading to enhanced singlet oxygen production at the porphyrin ligand upon irradiation. While this work required multiple steps to achieve the desired surface modification, it is a compelling demonstration of the power of direct coordination to labile surface metal sites, and highly orthogonal organic click chemistry to install complex, programmable ligands.

Importantly, this general approach is not limited to carboxylate-terminated ligands. For example, nitrogen-bearing ligands have been demonstrated as useful coordinating moieties for ligand installation.[77] Granick and co-workers showed that an imidazolate-modified BODIPY dye could be functionalized onto the surface of ZIF-8 (Zn_2(methylimidazolate) via surface ligand exchange under relatively mild conditions.[54] Confocal microscopy was employed to verify that the scope of functionalization

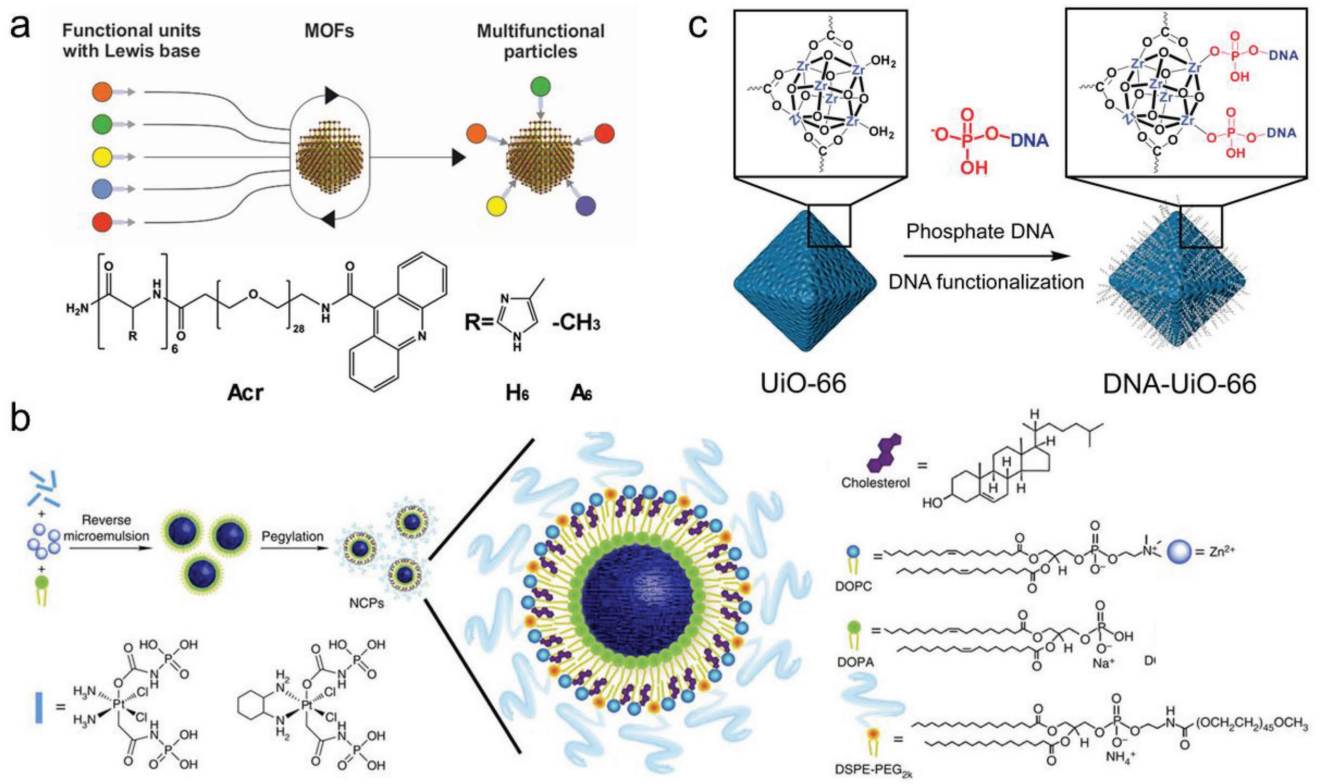

Figure 5. Schematic representation of postsynthetic external surface functionalization via different coordinative interactions. a) MOF NPs functionalized with diverse surface ligands via chelation of SBUs with datively bound histidine (imidazole) units (panel (a), bottom). Reproduced with permission.[78] Copyright 2017, American Chemical Society. b) Zinc bisphosphonate NCPs functionalized with DOPA, and assembled into asymmetric lipid bilayers via hydrophobic–hydrophobic interactions between DOPA and DOPC/cholesterol/DSPE-PEG_{2k} (bottom right). Reproduced with permission.[79c] Copyright 2014, Nature Publishing Group. c) Oligonucleotide modification of UiO-66 MOF NPs utilizing terminal phosphate-modified DNA. Reproduced with permission.[85] Copyright 2017, American Chemical Society.

was limited to the particle surface, as predicted by the relative size of the BODIPY dye and the narrow pores of the ZIF-8 MOF. The amine-based coordinative ligand was further improved by Lächelt and co-workers, who developed a versatile oligohistidine tag-based coordination strategy to immobilize a series of peptides and proteins onto three archetypical carboxylate-based MOF NPs: MIL-88A-Fe, HKUST-1, and Zr–fum (**Figure 5**a).[78] In this report, surface exchange of the nitrogen-based ligands was ensured by designing the ligand in such a way that two histidine groups would cooperatively chelate individual surface metal atoms. This chelation strategy proved highly successful, yielding dense surface coverage and allowing for explorations of cellular uptake coinciding with peptide and protein delivery.

While the aforementioned systems employ ligand modifications that closely mimic the coordinating moieties of the framework linkers, phosphate units have shown great promise in PSM surface functionalization. In a series of studies, Lin and co-workers elegantly showed that a monolayer of phosphate-terminated lipids could be attached to MOF and nanoscale coordination polymer (NCP) external surfaces.[79] Intriguingly, a second layer of lipid molecules could be subsequently coated onto the lipid-terminated particles to form asymmetric lipid bilayers, a process driven by hydrophobic–hydrophobic interactions. With this approach, Lin and co-workers developed the first self-assembled NCP for the delivery of the anticancer prodrug cisplatin (Figure 5b).[79c] The authors employed a microemulsion technique to synthesize Zn NCPs in the presence of 1,2-dioleoyl-*sn*-glycero-3-phosphate sodium salt (DOPA), a phosphate-terminated lipid that coordinates strongly to the surface zinc atoms of the NCPs. The DOPA-coated NCPs were then coated with 1,2-dioleoyl-*sn*-glycero-3-phosphocholine (DOPC), cholesterol, and 1,2-distearoyl-*sn*-glycero-3-phosphoethanolamine-*N*-[methoxy(polyethyleneglycol)-2000] (DSPE-PEG_{2k}) in a 4:4:2 molar ratio via hydrophobic interactions, leading to self-assembled asymmetric lipid bilayers. In addition to coordination chemistry approaches, external surface functionalization with lipids has also been achieved through electrostatic interactions and solvent-exchange deposition strategies.[79a,80] For example, with the goal of developing new nanoscale drug delivery vehicles for cancer treatment, Wuttke and co-workers reported the encapsulation of Fe-MIL-88A NPs within exosomes, which are endogenous cell-derived vesicles composed of phospholipid bilayers.[81] The encapsulation of drug-loaded MOF NPs was realized using the fusion method, as developed by Liu et al.,[82] leading to a versatile drug delivery vehicle with efficient cell uptake and no premature leakage. Surface functionalization with lipid bilayers offers several advantages: 1) stabilizing the NPs and facilitating their internalization into cells,[80] 2) decreasing cargo release rate,[79a] and 3) improving the

chemical tailorability of MOF NP due to the diverse range of lipid bilayer compositions available.[83]

Moving away from amorphous NCPs, Mirkin and co-workers recently used this approach to demonstrate the PSM of crystalline UiO MOF NPs with phosphate-terminated lipids through a one-step phase transfer reaction at room temperature.[84] In addition to phospholipids, Mirkin and co-workers functionalized a large series of MOF NPs with phosphate-terminated oligonucleotides (Figure 5c).[85] They showed that a high density of DNA could be appended to NPs of nine archetypical MOFs, yielding a library of oligonucleotide-functionalized MOF NP conjugates. This study revealed design rules for functionalizing MOF NPs with nucleic acids such as surface coverage positively correlates with surface SBU density, SBU coordination number, and metal–phosphate bonding strength. This insight represented a significant advancement in the rational design and synthesis of MOF NP–nucleic acid conjugates. The use of phosphate ligands proved judicious, as: 1) strong phosphate coordination promotes exchange at surface sites under mild conditions, 2) the strength of phosphate coordination does not disturb the structure of the MOF, and 3) the introduction of phosphorus provides a spectroscopic handle (e.g., NMR and inductively coupled plasma optical emission spectrometry spectroscopy) for quantification of ligand surface coverage.

Collectively, these advances in the realm of PSM through covalent and coordinative bonds paved the way toward addressing some of the major challenges in surface functionalization of MOF NPs. These studies demonstrated enhanced control over surface ligand density, MOF NP colloidal stability, and modular design of functional MOF NP architectures that show promise for a variety of biomedical applications.

4. Future Directions and Applications

Herein, we summarized recent advances in synthetic strategies to obtain modular MOF NPs with control over particle size, shape, and surface chemistry. Through these advances, and additional improvements in synthesis and characterization methodologies, MOF NPs will emerge as a promising new class of functional nanomaterials with the potential to significantly impact the fields of catalysis,[5] separations,[86] and nanomedicine.[16f] Although remarkable progress has been made, there remains significant room for improvement in the understanding of key features of MOF NP synthesis and functionalization. In particular, explanations of the initial mechanisms of particle nucleation and how factors such as modulators, temperature, and solvent affect these primary events remain mainly postulational. As such, improved characterization and mechanistic understanding of nucleation and subsequent crystal growth will drastically improve our ability to convert MOF NP synthesis from empirically driven guesswork to a highly predictable science. Further, improving upon the capability to predictably synthesize MOF NPs of desired sizes from 10 to 200 nm, with high uniformity, should remain an important goal for this field. NPs of this size regime are particularly attractive for two main reasons: 1) fast substrate diffusion kinetics associated with large external surface area for site-isolated catalysis, and 2) size-dependent bioavailability (including with respect to cellular uptake, cytotoxicity, and blood circulation) for applications as biological probes and perhaps even for therapeutic agents. Potential advances in these areas include the continued evolution of strategies to effectively separate nucleation and growth processes, and the development of seed-mediated MOF NP synthetic approaches.[87] Beyond gaining a firmer understanding of particle growth, other opportunities for impactful contributions to this field include: improving diffraction-based techniques (i.e., X-ray and electron diffraction) for in situ characterization and in depth structural analysis of MOF NPs, modulating the chemical stability MOF NPs via surface functionalization (especially toward water and excess phosphate, which is currently lacking), developing MOF NPs with large pores (>3 nm) capable of encapsulating and delivering biomolecules,[88] and systematically evaluating MOF NP toxicity and pharmacokinetics in vivo.[16k,89]

To date, much of the focus in developing MOF NPs has been on medicinal applications, however, another exciting avenue is the use of MOF NP as the building blocks in mixed-matrix membranes and colloidal crystal engineering of ordered 3D metamaterials and devices.[90] For instance, incorporating uniform MOF NPs into membranes could maximize their potential separation and catalysis capabilities, taking advantage of the extremely high external surface areas of MOF NPs and the attractive mechanical properties (stretchability, elasticity, and toughness) of polymeric matrices.[91] Such combinations will inevitably lead to a rich spectrum of material properties and functionalities, in part due to the tunable chemistry of MOFs as well as polymers. Specifically, we anticipate a diverse range of MOF NP-derived stimuli-responsive materials will emerge as important building components for flexible sensors, adaptive membranes, and artificial skin. Moreover, hierarchical materials composed of self-assembled MOF NP building blocks are hypothesized to exhibit properties unique from those demonstrated with conventional inorganic NPs owing to their porosity, tailorable host–guest interactions, and chemical and physical modularities. For example, photonic crystals and optoelectronic devices may result from the combination of guest molecules coupled with 3D ordered arrays of MOF NPs.[55,92] Thus far, few examples of ordered structures have been prepared from MOF NP building blocks, all of which are entropically driven to form closed packed assemblies.[53b,c,93] On the contrary, enthalpically driven assembly strategies are predictable and modular tools for assembling inorganic NPs into a huge library of well-defined architectures.[94] This has been primarily achieved through surface functionalization of NP building blocks with programmable ligands, such as oligonucleotides, which gives access to tunable interparticle distances, enthalpically favored topologies, and hybrid superstructures containing multiple functional units.[95] In this vein, significant opportunities remain open for exploration including: 1) systematic modulation of facet–facet interactions between MOF NP building blocks, 2) establishment of design rules for assembling MOF NPs into hierarchically ordered structures, and 3) incorporation of MOF NPs into stimuli-responsive metamaterials for sensing and catalysis applications. [96]

The modular synthesis of chemically addressable nanomaterials, such as MOF NPs, represents a powerful approach to realize desirable functionalities based on rational design and

bottom-up assembly of molecular components. We believe that research on MOF NPs can lead to a new generation of smart materials that offer solutions to important issues concerning energy, the environment, and human health.

Acknowledgements

This material was based upon work supported by the following awards: Air Force Office of Scientific ResearchFA9550-14-1-0274 and FA9550-17-1-0348, U.S. ArmyW911NF-15-1-0151, and National Science FoundationCHE-1709888. S.W. acknowledges support from a PPG fellowship. A.d. acknowledges a National Science Foundation Graduate Research Fellowship.

Conflict of Interest

The authors declare no conflict of interest.

Keywords

metal-organic frameworks, modular nanomaterials, nanoparticle syntheses, surface functionalization

Received: January 9, 2018
Revised: February 13, 2018
Published online:

[1] a) O. M. Yaghi, M. O'Keeffe, N. W. Ockwig, H. K. Chae, M. Eddaoudi, J. Kim, *Nature* **2003**, *423*, 705; b) S. Kitagawa, R. Kitaura, S. Noro, *Angew. Chem., Int. Ed.* **2004**, *43*, 2334; c) G. Ferey, *Chem. Soc. Rev.* **2008**, *37*, 191.
[2] M. Eddaoudi, J. Kim, N. Rosi, D. Vodak, J. Wachter, M. O'Keeffe, O. M. Yaghi, *Science* **2002**, *295*, 469.
[3] L. E. Kreno, J. T. Hupp, R. P. Van Duyne, *Anal. Chem.* **2010**, *82*, 8042.
[4] T. H. Bae, J. S. Lee, W. L. Qiu, W. J. Koros, C. W. Jones, S. Nair, *Angew. Chem., Int. Ed.* **2010**, *49*, 9863.
[5] J. Lee, O. K. Farha, J. Roberts, K. A. Scheidt, S. T. Nguyen, J. T. Hupp, *Chem. Soc. Rev.* **2009**, *38*, 1450.
[6] P. Horcajada, T. Chalati, C. Serre, B. Gillet, C. Sebrie, T. Baati, J. F. Eubank, D. Heurtaux, P. Clayette, C. Kreuz, J. S. Chang, Y. K. Hwang, V. Marsaud, P. N. Bories, L. Cynober, S. Gil, G. Ferey, P. Couvreur, R. Gref, *Nat. Mater.* **2010**, *9*, 172.
[7] a) Y. Sakata, S. Furukawa, M. Kondo, K. Hirai, N. Horike, Y. Takashima, H. Uehara, N. Louvain, M. Meilikhov, T. Tsuruoka, S. Isoda, W. Kosaka, O. Sakata, S. Kitagawa, *Science* **2013**, *339*, 193; b) M. Sindoro, N. Yanai, A. Y. Jee, S. Granick, *Acc. Chem. Res.* **2014**, *47*, 459.
[8] J. M. Yang, Q. Liu, W. Y. Sun, *Microporous Mesoporous Mater.* **2014**, *190*, 26.
[9] T. Kiyonaga, M. Higuchi, T. Kajiwara, Y. Takashima, J. G. Duan, K. Nagashima, S. Kitagawa, *Chem. Commun.* **2015**, *51*, 2728.
[10] J. Park, Q. Jiang, D. W. Feng, L. Q. Mao, H. C. Zhou, *J. Am. Chem. Soc.* **2016**, *138*, 3518.
[11] M. A. Boles, D. Ling, T. Hyeon, D. V. Talapin, *Nat. Mater.* **2016**, *15*, 141.
[12] N. Stock, S. Biswas, *Chem. Rev.* **2012**, *112*, 933.
[13] K. K. Tanabe, S. M. Cohen, *Chem. Soc. Rev.* **2011**, *40*, 498.
[14] P. Hirschle, T. Preiß, F. Auras, A. Pick, J. Völkner, D. Valdepérez, G. Witte, W. J. Parak, J. O. Rädler, S. Wuttke, *CrystEngComm* **2016**, *18*, 4359.
[15] a) S. Hermes, T. Witte, T. Hikov, D. Zacher, S. Bahnmuller, G. Langstein, K. Huber, R. A. Fischer, *J. Am. Chem. Soc.* **2007**, *129*, 5324; b) J. Cravillon, C. A. Schröder, R. Nayuk, J. Gummel, K. Huber, M. Wiebcke, *Angew. Chem., Int. Ed.* **2011**, *50*, 8067; c) J. P. Patterson, P. Abellan, M. S. Denny, C. Park, N. D. Browning, S. M. Cohen, J. E. Evans, N. C. Gianneschi, *J. Am. Chem. Soc.* **2015**, *137*, 7322; d) Y. H. Zhu, J. Ciston, B. Zheng, X. H. Miao, C. Czarnik, Y. C. Pan, R. Sougrat, Z. P. Lai, C. E. Hsiung, K. X. Yao, I. Pinnau, M. Pan, Y. Han, *Nat. Mater.* **2017**, *16*, 532.
[16] a) A. M. Spokoyny, D. Kim, A. Sumrein, C. A. Mirkin, *Chem. Soc. Rev.* **2009**, *38*, 1218; b) A. Carne, C. Carbonell, I. Imaz, D. Maspoch, *Chem. Soc. Rev.* **2011**, *40*, 291; c) Q. L. Zhu, Q. Xu, *Chem. Soc. Rev.* **2014**, *43*, 5468; d) C. V. McGuire, R. S. Forgan, *Chem. Commun.* **2015**, *51*, 5199; e) C. Doonan, R. Riccò, K. Liang, D. Bradshaw, P. Falcaro, *Acc. Chem. Res.* **2017**, *50*, 1423; f) C. B. He, D. M. Liu, W. B. Lin, *Chem. Rev.* **2015**, *115*, 11079; g) S. Dang, Q. L. Zhu, Q. Xu, *Nat. Rev. Mater.* **2017**, *3*, 17075; h) S. Furukawa, J. Reboul, S. Diring, K. Sumida, S. Kitagawa, *Chem. Soc. Rev.* **2014**, *43*, 5700; i) S. Wuttke, M. Lismont, A. Escudero, B. Rungtaweevoranit, W. J. Parak, *Biomaterials* **2017**, *123*, 172; j) M. Lismont, L. Dreesen, S. Wuttke, *Adv. Funct. Mater.* **2017**, *27*, 1606314; k) M. Gimenez-Marques, T. Hidalgo, C. Serre, P. Horcajada, *Coord. Chem. Rev.* **2016**, *307*, 342.
[17] J. Cravillon, R. Nayuk, S. Springer, A. Feldhoff, K. Huber, M. Wiebcke, *Chem. Mater.* **2011**, *23*, 2130.
[18] N. T. K. Thanh, N. Maclean, S. Mahiddine, *Chem. Rev.* **2014**, *114*, 7610.
[19] S. Surble, F. Millange, C. Serre, G. Ferey, R. I. Walton, *Chem. Commun.* **2006**, 1518.
[20] a) V. K. Lamer, R. H. Dinegar, *J. Am. Chem. Soc.* **1950**, *72*, 4847; b) W. Ostwald, *Z. Phys. Chem.* **1900**, *34*, 495.
[21] W. B. Lin, W. J. Rieter, K. M. L. Taylor, *Angew. Chem., Int. Ed.* **2009**, *48*, 650.
[22] X. P. Sun, S. J. Dong, E. K. Wang, *J. Am. Chem. Soc.* **2005**, *127*, 13102.
[23] a) M. Oh, C. A. Mirkin, *Nature* **2005**, *438*, 651; b) M. Oh, C. A. Mirkin, *Angew. Chem., Int. Ed.* **2006**, *45*, 5492.
[24] W. J. Rieter, K. M. Pott, K. M. L. Taylor, W. B. Lin, *J. Am. Chem. Soc.* **2008**, *130*, 11584.
[25] J. Klinowski, F. A. A. Paz, P. Silva, J. Rocha, *Dalton Trans.* **2011**, *40*, 321.
[26] Z. Ni, R. I. Masel, *J. Am. Chem. Soc.* **2006**, *128*, 12394.
[27] T. Chalati, P. Horcajada, R. Gref, P. Couvreur, C. Serre, *J. Mater. Chem.* **2011**, *21*, 2220.
[28] Y. S. Li, H. Bux, A. Feldhoff, G. L. Li, W. S. Yang, J. Caro, *Adv. Mater.* **2010**, *22*, 3322.
[29] G. A. D. Briggs, *Interdiscip. Sci. Rev.* **1990**, *15*, 190.
[30] K. S. Suslick, *Science* **1990**, *247*, 1439.
[31] E. Haque, N. A. Khan, J. H. Park, S. H. Jhung, *Chem. - Eur. J.* **2010**, *16*, 1046.
[32] N. A. Khan, S. H. Jhung, *Coord. Chem. Rev.* **2015**, *285*, 11.
[33] a) S. H. Jhung, J. H. Lee, J. W. Yoon, C. Serre, G. Ferey, J. S. Chang, *Adv. Mater.* **2007**, *19*, 121; b) K. M. L. Taylor-Pashow, J. Della Rocca, Z. G. Xie, S. Tran, W. B. Lin, *J. Am. Chem. Soc.* **2009**, *131*, 14261; c) N. A. Khan, I. J. Kang, H. Y. Seok, S. H. Jhung, *Chem. Eng. J.* **2011**, *166*, 1152; d) M. Y. Ma, A. Betard, I. Weber, N. S. Al-Hokbany, R. A. Fischer, N. Metzler-Nolte, *Cryst. Growth Des.* **2013**, *13*, 2286; e) N. A. Khan, E. Haque, S. H. Jhung, *Phys. Chem. Chem. Phys.* **2010**, *12*, 2625.
[34] J. Eastoe, M. J. Hollamby, L. Hudson, *Adv. Colloid Interface Sci.* **2006**, *128*, 5.

[35] W. J. Rieter, K. M. L. Taylor, H. Y. An, W. L. Lin, W. B. Lin, *J. Am. Chem. Soc.* **2006**, *128*, 9024.
[36] K. M. L. Taylor, W. J. Rieter, W. B. Lin, *J. Am. Chem. Soc.* **2008**, *130*, 14358.
[37] X. J. Zhao, X. L. Fang, B. H. Wu, L. S. Zheng, N. F. Zheng, *Sci. China: Chem.* **2014**, *57*, 141.
[38] a) M. L. Pang, A. J. Cairns, Y. L. Liu, Y. Belmabkhout, H. C. Zeng, M. Eddaoudi, *J. Am. Chem. Soc.* **2013**, *135*, 10234; b) X. C. Cai, X. R. Deng, Z. X. Xie, S. X. Bao, Y. S. Shi, J. Lin, M. L. Pang, M. Eddaoudi, *Chem. Commun.* **2016**, *52*, 9901.
[39] A. Carne-Sanchez, I. Imaz, M. Cano-Sarabia, D. Maspoch, *Nat. Chem.* **2013**, *5*, 203.
[40] R. Ameloot, F. Vermoortele, W. Vanhove, M. B. J. Roeffaers, B. F. Sels, D. E. De Vos, *Nat. Chem.* **2011**, *3*, 382.
[41] J. Cravillon, S. Munzer, S. J. Lohmeier, A. Feldhoff, K. Huber, M. Wiebcke, *Chem. Mater.* **2009**, *21*, 1410.
[42] B. Seoane, A. Dikhtiarenko, A. Mayoral, C. Tellez, J. Coronas, F. Kapteijn, J. Gascon, *CrystEngComm* **2015**, *17*, 1693.
[43] a) T. Uemura, S. Kitagawa, *J. Am. Chem. Soc.* **2003**, *125*, 7814; b) T. Uemura, Y. Hoshino, S. Kitagawa, K. Yoshida, S. Isoda, *Chem. Mater.* **2006**, *18*, 992.
[44] W. Cho, H. J. Lee, M. Oh, *J. Am. Chem. Soc.* **2008**, *130*, 16943.
[45] T. Tsuruoka, S. Furukawa, Y. Takashima, K. Yoshida, S. Isoda, S. Kitagawa, *Angew. Chem., Int. Ed.* **2009**, *48*, 4739.
[46] a) S. Diring, S. Furukawa, Y. Takashima, T. Tsuruoka, S. Kitagawa, *Chem. Mater.* **2010**, *22*, 4531; b) A. Umemura, S. Diring, S. Furukawa, H. Uehara, T. Tsuruoka, S. Kitagawa, *J. Am. Chem. Soc.* **2011**, *133*, 15506.
[47] a) M. Hu, S. Furukawa, R. Ohtani, H. Sukegawa, Y. Nemoto, J. Reboul, S. Kitagawa, Y. Yamauchi, *Angew. Chem., Int. Ed.* **2012**, *51*, 984; b) M. Hu, A. A. Belik, M. Imura, Y. Yamauchi, *J. Am. Chem. Soc.* **2013**, *135*, 384.
[48] C. Avci, J. Arinez-Soriano, A. Carne-Sanchez, V. Guillerm, C. Carbonell, I. Imaz, D. Maspoch, *Angew. Chem., Int. Ed.* **2015**, *54*, 14417.
[49] E. D. Bloch, W. L. Queen, R. Krishna, J. M. Zadrozny, C. M. Brown, J. R. Long, *Science* **2012**, *335*, 1606.
[50] A. Schaate, P. Roy, A. Godt, J. Lippke, F. Waltz, M. Wiebcke, P. Behrens, *Chem. - Eur. J.* **2011**, *17*, 6643.
[51] G. C. Shearer, S. Chavan, S. Bordiga, S. Svelle, U. Olsbye, K. P. Lillerud, *Chem. Mater.* **2016**, *28*, 3749.
[52] W. Morris, S. Z. Wang, D. Cho, E. Auyeung, P. Li, O. K. Farha, C. A. Mirkin, *ACS Appl. Mater. Interfaces* **2017**, *9*, 33413.
[53] a) M. L. Pang, A. J. Cairns, Y. L. Liu, Y. Belmabkhout, H. C. Zeng, M. Eddaoudi, *J. Am. Chem. Soc.* **2012**, *134*, 13176; b) M. Tsotsalas, A. Umemura, F. Kim, Y. Sakata, J. Reboul, S. Kitagawa, S. Furukawa, *J. Mater. Chem.* **2012**, *22*, 10159; c) G. Lu, C. L. Cui, W. N. Zhang, Y. Y. Liu, F. W. Huo, *Chem. - Asian J.* **2013**, *8*, 69.
[54] a) N. Yanai, S. Granick, *Angew. Chem., Int. Ed.* **2012**, *51*, 5638; b) N. Yanai, M. Sindoro, J. Yan, S. Granick, *J. Am. Chem. Soc.* **2013**, *135*, 34.
[55] C. Avci, I. Imaz, A. Carné-Sánchez, J. A. Pariente, N. Tasios, J. Pérez-Carvajal, M. I. Alonso, A. Blanco, M. Dijkstra, C. López, D. Maspoch, *Nat. Chem.* **2018**, *10*, 78.
[56] a) E. Biemmi, S. Christian, N. Stock, T. Bein, *Microporous Mesoporous Mater.* **2009**, *117*, 111; b) M. L. Kelty, W. Morris, A. T. Gallagher, J. S. Anderson, K. A. Brown, C. A. Mirkin, T. D. Harris, *Chem. Commun.* **2016**, *52*, 7854.
[57] a) C. B. Murray, C. R. Kagan, M. G. Bawendi, *Annu. Rev. Mater. Sci.* **2000**, *30*, 545; b) A. C. Templeton, M. P. Wuelfing, R. W. Murray, *Acc. Chem. Res.* **2000**, *33*, 27; c) A. Verma, F. Stellacci, *Small* **2010**, *6*, 12.
[58] a) F. Alexis, E. Pridgen, L. K. Molnar, O. C. Farokhzad, *Mol. Pharmaceutics* **2008**, *5*, 505; b) S. D. Li, L. Huang, *Mol. Pharmaceutics* **2008**, *5*, 496.
[59] N. Nakajima, Y. Ikada, *Bioconjugate Chem.* **1995**, *6*, 123.
[60] S. Jung, Y. Kim, S. J. Kim, T. H. Kwon, S. Huh, S. Park, *Chem. Commun.* **2011**, *47*, 2904.
[61] Y. H. Shih, S. H. Lo, N. S. Yang, B. Singco, Y. J. Cheng, C. Y. Wu, I. H. Chang, H. Y. Huang, C. H. Lin, *ChemPlusChem* **2012**, *77*, 982.
[62] P. H. Ling, J. P. Lei, L. Zhang, H. X. Ju, *Anal. Chem.* **2015**, *87*, 3957.
[63] S. M. Moghimi, A. C. Hunter, J. C. Murray, *Pharmacol. Rev.* **2001**, *53*, 283.
[64] A. Zimpel, T. Preiß, R. Röder, H. Engelke, M. Ingrisch, M. Peller, J. O. Rädler, E. Wagner, T. Bein, U. Lächelt, S. Wuttke, *Chem. Mater.* **2016**, *28*, 3318.
[65] O. Karagiaridi, W. Bury, J. E. Mondloch, J. T. Hupp, O. K. Farha, *Angew. Chem., Int. Ed. Engl.* **2014**, *53*, 4530.
[66] K. Xie, Q. Fu, Y. He, J. Kim, S. J. Goh, E. Nam, G. G. Qiao, P. A. Webley, *Chem. Commun.* **2015**, *51*, 15566.
[67] S. Nagata, K. Kokado, K. Sada, *Chem. Commun.* **2015**, *51*, 8614.
[68] Y. Goto, H. Sato, S. Shinkai, K. Sada, *J. Am. Chem. Soc.* **2008**, *130*, 14354.
[69] a) C. M. Calabrese, T. J. Merkel, W. E. Briley, P. S. Randeria, S. P. Narayan, J. L. Rouge, D. A. Walker, A. W. Scott, C. A. Mirkin, *Angew. Chem., Int. Ed.* **2015**, *54*, 476; b) W. Morris, W. E. Briley, E. Auyeung, M. D. Cabezas, C. A. Mirkin, *J. Am. Chem. Soc.* **2014**, *136*, 7261.
[70] J. I. Cutler, E. Auyeung, C. A. Mirkin, *J. Am. Chem. Soc.* **2012**, *134*, 1376.
[71] a) J. S. Kahn, L. Freage, N. Enkin, M. A. A. Garcia, I. Willner, *Adv. Mater.* **2017**, *29*, 1602782; b) W. Chen, X. Yu, A. Cecconello, Y. S. Sohn, R. Nechushtai, I. Willner, *Chem. Sci.* **2017**, *8*, 5769.
[72] I. Abanades Lazaro, S. Haddad, S. Sacca, C. Orellana-Tavra, D. Fairen-Jimenez, R. S. Forgan, *Chem* **2017**, *2*, 561.
[73] C. B. He, K. D. Lu, D. M. Liu, W. B. Lin, *J. Am. Chem. Soc.* **2014**, *136*, 5181.
[74] D. Y. Hong, Y. K. Hwang, C. Serre, G. Ferey, J. S. Chang, *Adv. Funct. Mater.* **2009**, *19*, 1537.
[75] M. Kondo, S. Furukawa, K. Hirai, S. Kitagawa, *Angew. Chem., Int. Ed.* **2010**, *49*, 5327.
[76] L. He, M. Brasino, C. Mao, S. Cho, W. Park, A. P. Goodwin, J. N. Cha, *Small* **2017**, *13*, 1700504.
[77] Y. K. Hwang, D. Y. Hong, J. S. Chang, S. H. Jhung, Y. K. Seo, J. Kim, A. Vimont, M. Daturi, C. Serre, G. Ferey, *Angew. Chem., Int. Ed.* **2008**, *47*, 4144.
[78] R. Röder, T. Preiß, P. Hirschle, B. Steinborn, A. Zimpel, M. Höhn, J. O. Rädler, T. Bein, E. Wagner, S. Wuttke, U. Lächelt, *J. Am. Chem. Soc.* **2017**, *139*, 2359.
[79] a) D. M. Liu, S. A. Kramer, R. C. Huxford-Phillips, S. Z. Wang, J. Della Rocca, W. B. Lin, *Chem. Commun.* **2012**, *48*, 2668; b) C. B. He, D. M. Liu, W. B. Lin, *Biomaterials* **2015**, *36*, 124; c) D. M. Liu, C. Poon, K. D. Lu, C. B. He, W. B. Lin, *Nat. Commun.* **2014**, *5*, 4182; d) R. C. Huxford-Phillips, S. R. Russell, D. M. Liu, W. B. Lin, *RSC Adv.* **2013**, *3*, 14438.
[80] S. Wuttke, S. Braig, T. Preiß, A. Zimpel, J. Sicklinger, C. Bellomo, J. O. Rädler, A. M. Vollmar, T. Bein, *Chem. Commun.* **2015**, *51*, 15752.
[81] B. Illes, S. Wuttke, H. Engelke, *Nanomaterials* **2017**, *7*, 351.
[82] J. W. Liu, X. M. Jiang, C. Ashley, C. J. Brinker, *J. Am. Chem. Soc.* **2009**, *131*, 7567.
[83] B. Illes, P. Hirschle, S. Baenert, V. Cauda, S. Wuttke, H. Engelke, *Chem. Mater.* **2017**, *29*, 8042.
[84] S. Z. Wang, W. Morris, Y. Y. Liu, C. M. McGuirk, Y. Zhou, J. T. Hupp, O. K. Farha, C. A. Mirkin, *Angew. Chem., Int. Ed.* **2015**, *54*, 14738.
[85] S. Z. Wang, C. M. McGuirk, M. B. Ross, S. Y. Wang, P. C. Chen, H. Xing, Y. Liu, C. A. Mirkin, *J. Am. Chem. Soc.* **2017**, *139*, 9827.
[86] J. E. Bachman, Z. P. Smith, T. Li, T. Xu, J. R. Long, *Nat. Mater.* **2016**, *15*, 845.

[87] a) C. M. Doherty, D. Buso, A. J. Hill, S. Furukawa, S. Kitagawa, P. Falcaro, *Acc. Chem. Res.* **2014**, *47*, 396; b) H. Q. Xu, K. C. Wang, M. L. Ding, D. W. Feng, H. L. Jiang, H. C. Zhou, *J. Am. Chem. Soc.* **2016**, *138*, 5316; c) Y. F. Gu, Y. N. Wu, L. C. Li, W. Chen, F. T. Li, S. Kitagawa, *Angew. Chem., Int. Ed.* **2017**, *56*, 15658.

[88] a) K. Shen, L. Zhang, X. D. Chen, L. M. Liu, D. L. Zhang, Y. Han, J. Y. Chen, J. L. Long, R. Luque, Y. W. Li, B. L. Chen, *Science* **2018**, *359*, 206; b) K. Liang, R. Ricco, C. M. Doherty, M. J. Styles, S. Bell, N. Kirby, S. Mudie, D. Haylock, A. J. Hill, C. J. Doonan, P. Falcaro, *Nat. Commun.* **2015**, *6*, 7240.

[89] S. Wuttke, A. Zimpel, T. Bein, S. Braig, K. Stoiber, A. Vollmar, D. Muller, K. Haastert-Talini, J. Schaeske, M. Stiesch, G. Zahn, A. Mohmeyer, P. Behrens, O. Eickelberg, D. A. Bolukbas, S. Meiners, *Adv. Healthcare Mater.* **2017**, *6*, 1600818.

[90] a) P. Fratzl, R. Weinkamer, *Prog. Mater. Sci.* **2007**, *52*, 1263; b) S. Choi, T. Kim, H. Ji, H. J. Lee, M. Oh, *J. Am. Chem. Soc.* **2016**, *138*, 14434; c) J. W. Nai, B. Y. Guan, L. Yu, X. W. Lou, *Sci. Adv.* **2017**, *3*, e1700732.

[91] B. Seoane, J. Coronas, I. Gascon, M. E. Benavides, O. Karvan, J. Caro, F. Kapteijn, J. Gascon, *Chem. Soc. Rev.* **2015**, *44*, 2421.

[92] H. Bin Wu, X. W. Lou, *Sci. Adv.* **2017**, *3*, eaap9252.

[93] S. C. Glotzer, M. J. Solomon, *Nat. Mater.* **2007**, *6*, 557.

[94] M. Grzelczak, J. Vermant, E. M. Furst, L. M. Liz-Marzan, *ACS Nano* **2010**, *4*, 3591.

[95] a) S. Y. Park, A. K. R. Lytton-Jean, B. Lee, S. Weigand, G. C. Schatz, C. A. Mirkin, *Nature* **2008**, *451*, 553; b) D. Nykypanchuk, M. M. Maye, D. van der Lelie, O. Gang, *Nature* **2008**, *451*, 549; c) R. J. Macfarlane, B. Lee, M. R. Jones, N. Harris, G. C. Schatz, C. A. Mirkin, *Science* **2011**, *334*, 204; d) M. R. Jones, N. C. Seeman, C. A. Mirkin, *Science* **2015**, *347*, 1260901.

[96] a) D. Bradshaw, A. Garai, J. Huo, *Chem. Soc. Rev.* **2012**, *41*, 2344; b) J. F. Yao, H. T. Wang, *Chem. Soc. Rev.* **2014**, *43*, 4470; c) Q. H. Yang, Q. Xu, H. L. Jiang, *Chem. Soc. Rev.* **2017**, *46*, 4774.